High Power Beta Electron Device - Beyond Betavoltaics

William M. Ayers [a,*], Charles A. Gentile [b]

a. Ayers Group, 910 Route 27, Princeton , N.J. 08540
b. Princeton Plasma Physics Laboratory, 100 Stellarator Rd., Princeton, N.J. 08540

Abstract

Developing watt level power sources with beta emitting radioisotopes has been limited by the inability to utilize high energy (> 100 KeV) beta emitters at high radioisotope loadings without damaging the energy conversion materials. A new type of beta electron power source is described that removes those restrictions. The approach contains the radioisotope in a beta transparent titanium tube and confines beta electrons emitted through the tube wall to spiral trajectories around the tube with an axial magnetic field. The confined beta electrons dissipate energy though multiple interactions with surrounding excimer precursor gas atoms to efficiently generate photons. Photovoltaic cells convert the photons to electrical power. Since the beta electrons dissipate energy in the excimer precursor gas, the device can be loaded with more than 10^{13} Bq of radioisotope to generate 100 milliwatt to watt levels of electrical power without damaging the device materials or degrading its performance. The power source can use a variety of beta radioisotopes and scales by stacking the devices.

1. Introduction

Unattended, long-life power sources are needed for devices in isolated environments. These sources can power communications and sensor applications on undersea platforms, deep space vehicles, and other remote, dark locations. Powering such devices with beta electron emitting radioisotope sources rather than rechargeable batteries can decrease system weight, provide extremely low temperature operation, and increase system longevity.

Attempts to efficiently convert beta electron charge and kinetic energy into electrical power have been pursued for decades. However, these approaches capture only a very small fraction of the beta electron energy. A recent review describes one type of beta radioisotope power device, the betavoltaic cell [1]. In these devices, beta electrons are absorbed in a doped semiconductor material to produce electron-hole pairs. The electron-hole pairs are separated by a Schottky or PIN junction to produce electrical power. The devices have nanowatt to microwatt power output and very low conversion efficiencies. A major problem with betavoltaic cells is destruction of the semiconductor material from beta electron bombardment. This limits such cells to low energy beta emitters, such as tritium, and small quantities of radioisotope[2]. The low radioisotope loading limits the power output.

Another energy conversion approach relies on generating excimer light from noble gas atoms with alpha and beta particles emitted from fission by-products. Prelas and co-workers have investigated this approach [3,4]. The alpha and beta emitting materials in the form of aerosol powders or encapsulated particles are mixed with the noble gas. The excimer light emission is captured by a photovoltaic cell to generate power. Problems with this approach include the need for significant radiation shielding,

danger of the fission by-product materials escaping from the device, and disposal of the long half-life radioisotopes.

To overcome these limitations, the device illustrated in Figure 1 uses a sealed, replaceable beta electron transparent tube containing a radioisotope such as krypton-85 gas. Kr-85 is available from the off-gas produced by acid dissolution of spent nuclear fuel rods at reprocessing plants. Tonnes of Kr-85 are presently vented into the atmosphere annually. The Kr-85 beta electrons, with an average energy of 251 KeV, pass through the tube wall while the radioisotope gas remains inside. Two permanent magnets at the ends of the tube provide a uniform magnetic field parallel to the tube axis. The high velocity beta electrons emitted through the tube wall interact with the magnetic field through the Lorentz force (qVxB) to confine and collimate the electrons in helical or spiral trajectories around the tube. As shown in Figure 2, a photon transparent tube containing an excimer precursor gas surrounds the radioisotope tube such that the confined beta electrons have thousands of interactions with the precursor gas atoms to generate excimer photons. The photovoltaic panels positioned around the excimer tube convert the photons to electrical power.

Since the high energy beta electrons are magnetically confined to trajectories through the excimer precursor gas, the beta energy is only dissipated through interactions with the gas atoms and excimer photon generation. Thus, unlike betavoltaic cells, little or no damage is done to the device materials which in turn minimizes degradation of the device performance over time. This beta confinement method also allows the device to be loaded with thousands of times the amount of radioisotope possible with betavoltaic cells thereby greatly increasing the power output. In addition, magnetic field confinement of the beta electrons reduces external radiation shielding.

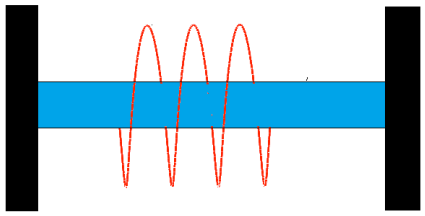

Fig.1. Helical trajectory of magnetically confined beta electrons emitted into a vacuum. The beta electrons are emitted through the thin walled titanium tube containing the radioisotope.

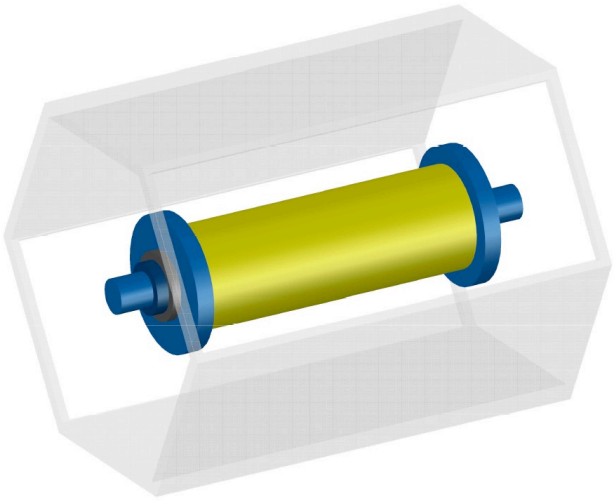

Fig. 2. Beta emitting tube (center) and surrounding excimer photon emitting tube inside a hexagonal enclosure with photovoltaic panels

The equations that govern the magnetically confined beta electron trajectories in both vacuum and the excimer precursor gas are presented in the following section. This is followed by a discussion of the beta interactions with the precursor gas, excimer generation efficiency, and the maximum excimer photon power output. Section 4 discusses beta electron energy losses from passing through the radioisotope tube and precursor gas that decrease the power output. Section 5 combines the equations developed in the previous sections to provide a general equation for the device electrical power output and summarizes device metrics for several radioisotope decay energies and loadings.

2. Beta Electron Trajectories in Vacuum

Beta emission is a random, isotropic process with straight line trajectories in the absence of external fields. In a magnetic field, the Lorentz force alters the beta paths into circular and helical trajectories depending on the beta emission angle with respect to the magnetic field. Trajectories in the excimer precursor gas, rather than vacuum, are discussed in Section 3.

The equation of motion for relativistic beta electrons with charge q(eV), rest mass m_o, and initial velocity V(m/sec) emitted into a uniform magnetic field, B(Tesla), is [5,6]:

(1) $$m_o \Upsilon (dV/dt) = q(VxB) = qBsin(\Phi)$$

Here Φ is the angle between the beta velocity vector and the magnetic field and Υ is the Lorentz factor::

(2) $$\Upsilon = 1/sqrt(1- (V^2/c^2))$$

where c is the speed of light.

The relationship between the beta electron initial velocity and radioisotope decay energy, KE, is:

(3) $KE = m_o c^2 (\Upsilon - 1)$

Such that:

(4) $V = c*sqrt(KE^2 + 2 KE*m_o c^2)/(KE + m_o c^2)$

The Beta velocity component parallel to the magnetic field is constant and the perpendicular component, $V_\perp$, changes with sin(Φ). The trajectory of beta electrons emitted perpendicular (90^o) to the magnetic field take on a circular trajectory and those with other emission angles have helical trajectories. For the 90^o emission angle, the cyclotron radius, R, is:

(5) $m_o V_\perp^2 / R = q V_\perp B$

(6) $R = m_o V_\perp / qB$ (meters)

Table 1 lists the respective cyclotron radii, velocities, and effective mass for Kr-85 and P-32 in a 0.2 T magnetic field. The radii and velocities are shown for both the average and maximum beta energies.

Table 1. Beta Electron Path Radii and Velocity in Vacuum

	Energy (KeV)	Velocity (% C)	Lorenz Υ	Velocity (m/sec)	Radius at 0.2 T (mm)
Kr-85	251(ave)	74.29	1.49	2.22E8	6.31
	687(max)	90.51	2.35	2.71E8	7.69
P-32	695	90.55	2.36	2.71E8	7.69
	1710	97.35	4.37	2.91E8	8.27

The beta trajectories at other emission angles are both right and left handed helices with radii:

(7) $R(\Phi) = m_o V / qB\sin(\Phi) = R/\sin(\Phi)$

Thus, for the various beta emission angles, there are multiple helical trajectories with different radii. The combined helical trajectories form a beta electron flux (beta electrons/cm2-sec) with a cross sectional area, A_β:

(8) $A_\beta = \pi (Rmax^2 - R^2)$ (cm^2)

Here R_{max} is determined from the average of integrating the helical radii, R/sin(Φ), over the range of emitted angles. For angles from 15 to 165 degrees, this average is 1.55 such that the average radius for this emission range is:

(9) $Rmax = 1.55*R$

Substituting Rmax into Eq. 8 yields:

(10) $A_\beta = 1.40*\pi*(m_o V_\perp/qB)^2$

The intensity, or number of beta electrons in the beta flux, is a function of the radioisotope specific activity, A(t), mass M (gm), and magnetic field, B(T):

(11) $J_{beta} = A(t)*M/A_\beta$ (beta/sec-cm^2)

(12) or $J_{beta} = A(t)*M/(1.55*\pi*(m_o V_\perp/qB)^2)$

Therefore, a major advantage of the device's axial magnetic field is that it collimates the beta trajectories into a focused beta electron flux. The beta flux, which is proportional to B^2, can be increased to enhance the excimer generation kinetics.

The radioisotope specific activity, in beta emissions per second per gram of radioisotope, is:

(13) $A(t)= Ao*\exp(- t/\tau)$ (beta/sec-gm)

with

(14) $Ao= (No/MW)*(\ln 2/t_{1/2})$ (beta/sec-gm)

and $\tau = t_{1/2}/\ln 2$

Here $t_{1/2}$ is the half-life of the radioisotope in seconds, Ao is its initial specific activity in beta emissions/sec-gm, No is 6.023 x 10^{23}, and MW is the radioisotope molecular weight. For Kr-85 with a half-life 10.75 years, its initial activity is 1.45 x 10^{13} beta/sec-gm or 1.45 x 10^{13} Bq/gm. This is also equal to 393 Ci/gm where 1 Ci is 3.7 x 10^{10} Bq. One Ci of beta emissions (3.7 x 10^{10} beta/sec) multiplied by the electron charge of 1.6x10^{-19} coulombs/beta provides 5.92 x10^{-9} coulombs/sec-Ci or the equivalent of 5.92 nanoamp/Ci of beta electron flux passing through the cross section area.

3. Excimer Photon Generation

The excimer photon generation rate with beta electrons can be estimated from electron gun studies of excimer generation. These studies determined that the excimer generation rate increases with precursor gas pressure, electron energy, and electron flux [7,8]. The efficiency of excimer photon power output to electron gun power input (current times acceleration voltage) ranges from 30% to 42% for 20 KV to 40 KV electron gun sources[9,10,11]. In the absence of data for higher electron energies, a 40% efficiency will also be assumed for the beta electron source.

The maximum power available from the beta electron source is:

(15) $P = A(t)*KE$ (watts/gm of radioisotope)

Here the specific activity, A(t), has units of beta /sec-gm and KE is the beta kinetic energy in joules/beta. The kinetic energy in joules is calculated from q*KeV (coulombs*volts).

For the Kr-85 beta electrons with an average decay energy of 251 KeV and initial activity of 1.45 x 10^{13} beta/sec-gm, the maximum power is 0.582 watts/gm of radioisotope.

Using the power efficiency from the electron gun beam studies, the average excimer power output is:

(16) $P_{ph} = A(t)*KE*\eta ex$ (photon watts/gm of radioisotope)

where ηex is the excimer power generation efficiency of 40%.

A more accurate calculation would integrate the power over all energies of the Kr-85 beta spectrum rather than using just the average energy. Fig. 3 shows the maximum excimer photon power output, P_{ph}, for average beta energies of 251 KeV and 187 KeV as a function the radioisotope loading in the titanium tube. As described in Section 5, 187 KeV is the average energy remaining after the beta electrons pass through the titanium tube.

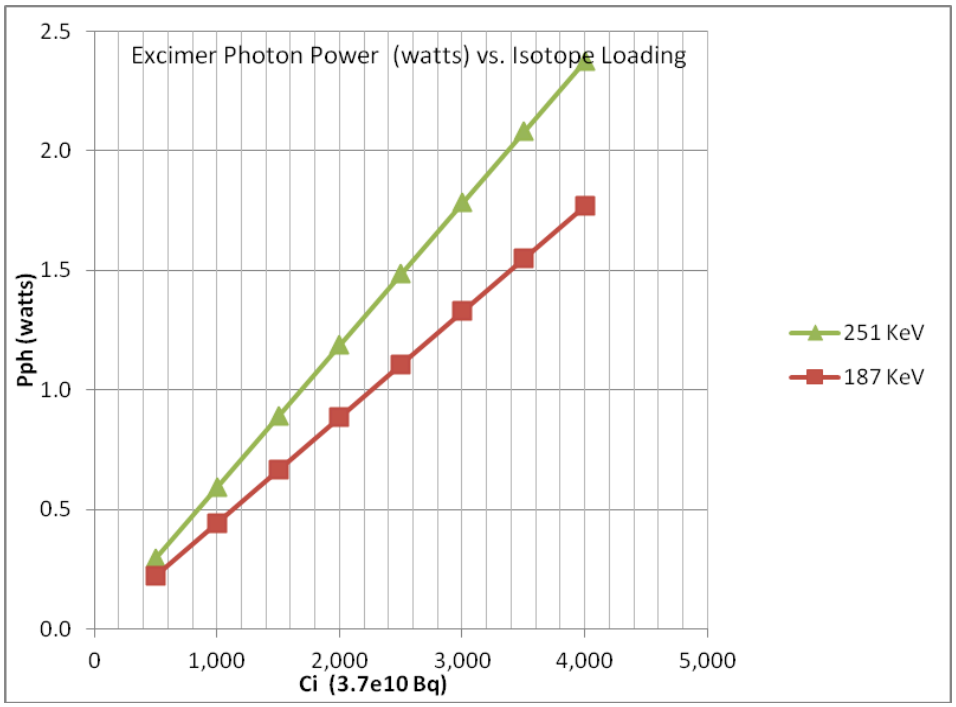

Fig. 3. Maximum excimer photon output power (watts) vs. radioisotope loading for ηex =0.4 (40%).

The number of beta electron interactions with precursor gas atoms, G, can be estimated from an energy balance of beta energy input, KE, to photon energy output, Eph.

(17) G = (KE/Eph)

The G ratios are listed in Table 3 for Kr-85 and P-32. For the Kr-85 average beta decay energy, the average ratio is 3 x 10^4. Also shown in the table are G ratios based on the average beta decay energy divided by the precursor gas first ionization energy.

Table 2. Precursor Gas and Excimer Energy

Excimer emitter	Eph, photon energy eV and (wavelength)	Precursor gas
Ar_2*	9.84 (126 nm)	Ar
Kr_2*	8.49 (146 nm)	Kr
Xe_2*	7.21 (172 nm)	Xe
ArF*	6.42 (193 nm)	Ar, NF_3
KrF*	5.01 (248 nm)	Kr, NF_3
XeCl*	4.03 (308 nm)	Xe, HCl
XeF*	3.53 (351 nm)	Xe, NF_3

Table 3 Numberof Photons Per Beta Electron Based on Energy Balance

Excimer emitters	Photon energy (eV) and wavelength (nm)	Ionization energy (eV)	Average Beta Energy	G Beta KeV/photon energy	G Beta KeV/ionization energy
Ar_2*	9.84 (126)	12.1	Kr-85@251KeV	2.6e4	2.1e4
			P-32@695KeV	7.1e4	5.7e4
Kr_2*	8.49 (146)	13.9	Kr-85@251KeV	2.9e4	1.8e4
			P-32@695KeV	8.1e4	5.0e4
Xe_2*	7.21 (172)	15.7	Kr-85@251KeV	3.5e4	1.6e4
			P-32@695KeV	9.6e4	4.4e4

4. Beta Energy Losses in the Precursor Gas and Radioisotope Tube

4.1 Energy Losses in the Precursor Gas

The theoretical maximum excimer power output shown in Fig. 3 is decreased by beta energy losses from passing through the precursor gas and titanium tube wall. The energy loss from passing through the gas can are estimated with NIST ESTAR Stopping Power data as a function of electron energy [12]. This energy loss in the gas, ΔKE_g, is calculated with

(18) $$\Delta KE_g = SP_g * \rho_g * x \quad \text{(MeV)}$$

or

(19) $$\Delta KE_g = SP_g * (MW*P/RT) * x$$

In these equations, SP_g is the gas total stopping power (MeV-cm^2/gm) and ρ_g is the gas density (gm/cm^3). Eq. 19 assumes ideal gas behavior where MW is the molecular weight, R, is the gas constant, T is temperature, and P is the gas pressure.

The total stopping power is the sum of the collision and radiation (Bremsstrahlung) stopping powers. Collision losses include coulomb interactions (excitation and ionization). Plotting the ESTAR collision and

radiation stopping data for argon and titanium in Fig. 4, shows that the radiation stopping power is significantly less that the collision stopping power (about 1 %) for beta energies less than 1 MeV.

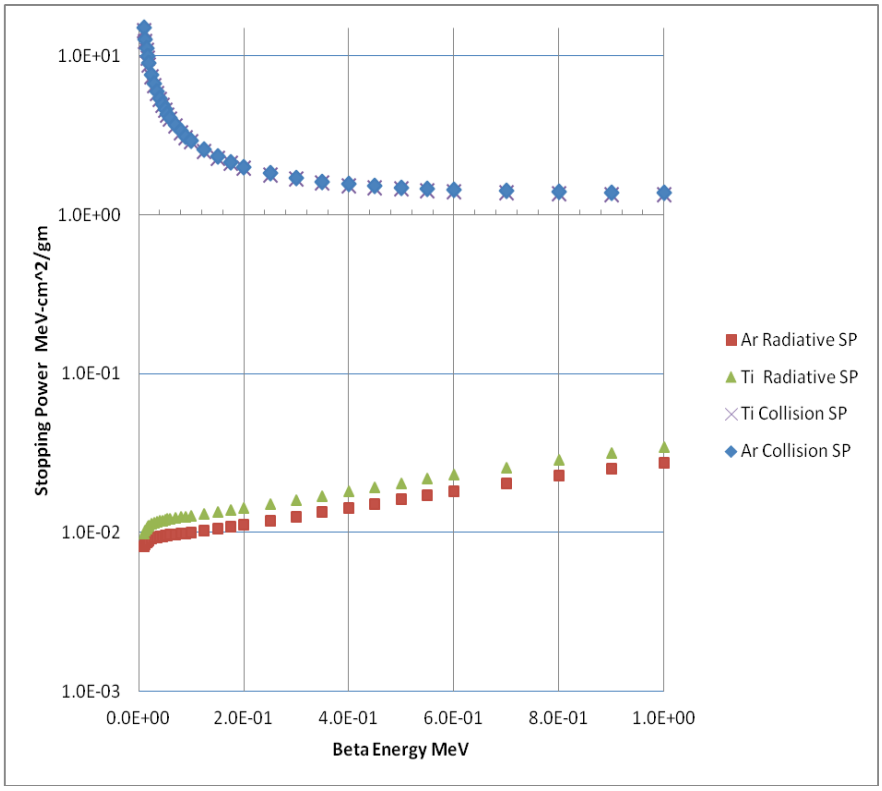

Fig. 4. Collision and Radiation Stopping Power for Argon and Titanium.

The total stopping power is used to calculate the energy loss, $\Delta KE_{g.}$, in the gases. These SP_g values for argon, krypton, and xenon are plotted in Fig. 5.

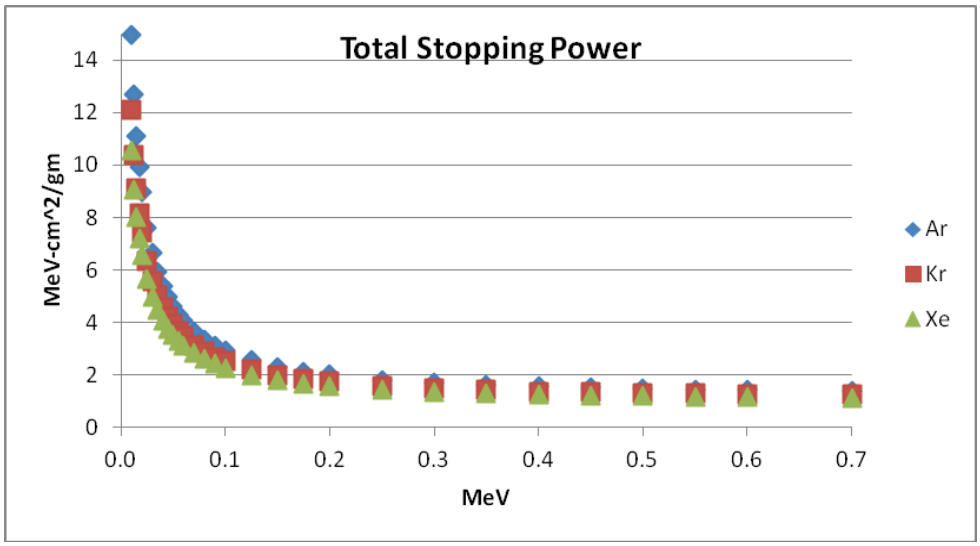

Fig. 5 Dependence of collision stopping power on beta electron energy for inert gases.

The stopping power data in Fig. 5 can be estimated with the power law equations listed in Table 4.

The equation for argon is:

(20) $SP_g(MeV) = 0.8947*MeV^{-0.57}$

As the beta electrons lose energy passing through the gas, the stopping power increases which further increases the rate of energy loss. For argon the energy loss is:

(21) $\Delta KE_g = 0.8947*MeV^{-0.57}*(1.781e-3)*x$

Evaluating Eq. 22 at 0.250 MeV, provides a ΔKE_g loss of 3.26 KeV over a one centimeter gas path length. There is little difference in the stopping powers for the gases. The difference in the energy losses, ΔKE_g, is mainly due to their respective gas densities.

Table4. Equations for Stopping Power and Derivative of Stopping Power with Energy

Gas	Gas Density	Stopping Power	$SPg*\rho_g$ at
		SPg(MeV)	0.250 MeV
	(gm/cm^3)	$MeV\text{-}cm^2/gm$	MeV/cm
Ar	1.781 e-3	$0.8947*MeV^{-0.57}$	3.26e-3
Kr	3.738e-3	$0.7991*MeV^{-0.552}$	6.02e-3
Xe	5.857e-3	$0.7499*MeV^{-0.54}$	8.71e-3

The distance required to dissipate all the beta energy in the gas determines the maximum beta trajectory length. This is calculated with the Continuous Slowing Down Approximation (CSDA) range data [12]. The CSDA range is the integral of the reciprocal of the total gas stopping power (radiation plus collision SP) as a function of energy. Table 5 lists the CSDA range factors and maximum beta trajectory distances, L, for several precursor gases at 250 KeV beta energy. The maximum beta trajectory distance is defined as:

(22) $L = CSDA/\rho_g = CSDA*RT/MW*P$ (cm)

This distance increases with temperature and decreases with increasing gas pressure. From the data in Table 4, and Eq. 22, the beta electrons travel about 50, 27, and 19 cm respectively in argon, krypton, and xenon at STP.

Table 5. Beta Electron CSDA Range Factors and Travel Distance Through Precursor Gases

Noble gas	Atomic mass	Density (gm/cm3)*	Excimer energy (eV)	Gas mean free path (cm)*	ESTAR CSDA range factor (gm/cm^2)	Kr-85 Beta Energy for ESTAR	Beta distance (cm)
				λ			L
Ar	39.94	1.781e-3	9.84	6.83e-6	0.0892	@251KeV	50.06
Kr	83.78	3.738e-3	8.49	5.23e-6	0.1028	@251KeV	27.50
Xe	131.29	5.857e-3	7.21	3.78e-6	0.1126	@251KeV	19.22

* at STP, 1 atmosphere, 273 K

The krypton CSDA range factor also controls the beta path length in the Kr-85 gas within the radioisotope tube. Increasing the Kr-85 pressure inside the tube will shorten L. From Eq. 22 and Table 5, increasing the Kr-85 pressure to 20 atmospheres at 273K would decrease the maximum beta distance, L, to 1.37 cm. Depending on the tube diameter, this smaller beta path length could decrease the number of beta electrons passing through the tube wall and into the precursor gas. Another issue for the Kr-85 inside the radioisotope tube is that the Kr-85 gas decays into Rb-85 metal atoms. This decreases the Kr-85 pressure in the tube over time. The drop in pressure is proportional to the change in Kr-85 activity, A(t). Hence the pressure decreases as exp(- t/τ). The pressure drop will also increase the CSDA value and increase the beta transit distance through the gas.

The CSDA methodology assumes a linear decrease in electron kinetic energy with distance. With this assumption, the beta kinetic energy decrease through the gas is:

(23) $$KE(x)= KE\ (1-x/L)$$

Substituting Eq. 22 for L yields:

(24) $$KE(x)= KE\ (1-x/(CSDA*RT/MW*P))$$

4.2 Beta Energy Losses in the Titanium Radioisotope Tube

The beta electron energy loss from passing through the titanium tube wall is also estimated with the NIST ESTAR Stopping Power data [12]. The energy loss for the titanium tube, ΔKE_m, is:

(25) $$\Delta KE_m = SP_m * \rho_m * T_m / \sin(\Phi)$$

where SP_m is the metal stopping power, ρ_m the density, and Tm is the tube wall thickness. The titanium stopping power is 1.83 MeV-cm^2/gm for 250KeV electrons and the density is 4.5 gm/cm^3 . Hence, the energy loss per cm, $SP_m * \rho_m$, is 8.2 MeV/cm. The titanium stopping power as a function of beta energy up to 1 MeV, can be calculated with [12]:

(26) $$SP_m(MeV)= 1.203*MeV^{-0.463}$$

The beta energy lost through the tube is also a function of the beta emission angle through the tube wall as shown in Fig. 6. The beta path length through the wall increases as $T_m/\sin(\Phi)$. For a 90^o emission angle relative to the tube axis, the minimum beta path is equal to the wall thickness, Tm. Substituting a wall thickness of 0.005cm in Eq. 25 yields the minimum ΔKE_m wall energy loss of 41 KeV. This is about 16% of the 251KeV initial energy.

As shown in Fig. 6, emission angles less than 15^o or greater than 165^o result in more than 62% of the beta kinetic energy lost in the tube wall because of the longer path lengths. Emission angles less than 10^o or greater than 170^o have more than a 93% loss. Averaging the integral of $T_m/\sin(\Phi)$ over allowable emission angles provides an average tube wall beta path length. For emission angles between 15 to 165 degrees (0.261 to 2.879 radians), this averaged path length is 1.55 Tm. With this average value, Eq. 25 is simplified to:

(27) $$\Delta KE_m = 1.55*SP_m*\rho_m*T_m$$

These substitutions yield the averaged beta energy loss, ΔKE_m, of 1.55*41 KeV or 63.5 KeV.

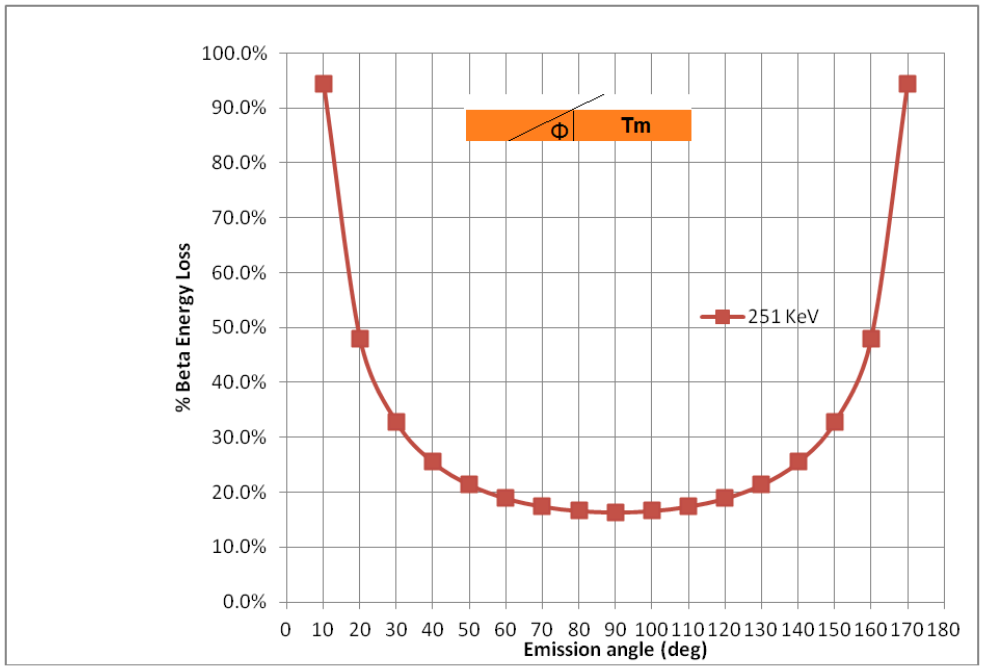

Fig. 6. Percent beta energy loss $\Delta KE_m/KE$ through tube wall versus emission angle,

With this beta energy loss , the remaining beta kinetic energy, KE_n, after the passing through the tube wall is:

(28) $KE_n = (KE - SP_m * \rho_m * T_m / \sin(\Phi))$

or:

(29) $KE_n = (KE - 1.55 * SP_m * \rho_m * T_m)$

for beta emission angles between 15 and 165 degrees. For a Tm thickness of 0.005cm and an initial KE of 251 KeV, KE_n is 251-63.5 or about 187 KeV.

In addition to the kinetic energy loss as beta electrons pass through the tube walls, the number of electrons that pass through the walls and into the precursor gas is also decreased. This reduction can be estimated by multiplying the initial activity, A(t) by the allowable emission angles through the tube walls. Dividing those angles, Φ_{max} and Φ_{min}, by the 360^o range of emission angles above and below the tube axis provide the ratio:

(30) $B\% = 2*(\Phi_{max} - \Phi_{min})/360$

such that the reduced number of beta electrons ,A_n, emitted into the precursor gas are:

(31) $A_n(t) = A(t)*B\%$ (beta/gm-sec)

For example, with a Φ_{max} of 165 and Φ_{min} of 15 degrees, B% is 83.3% and $A_n(t)$ is 0.833*A(t).

The final corrected kinetic energy equation, after including the precursor gas and tube beta energy loss terms, is shown in Eq. 32. The corrected energy equation is a function of the initial decay energy, tube wall thickness, emission angle, metal stopping power, CSDA for the gas, distance travelled through the gas, gas pressure,and temperature.

(32) $$KEn = (KE - (SP_m * \rho_m * T_m / \sin(\Phi)) * [1 - (x/(CSDA * RT/MW * P)]$$

For emission angles 15 to 165 degrees Eq. 32 simplifies to:

(33) $$KEn(x) = (KE - 1.55 * SP_m * \rho_m * T_m) * [1 - (x/(CSDA * RT/MW * P)]$$

4. 3 Beta Velocity and Time of Flight Through the Precursor Gas:

With Eq. 33, the velocity as a function of kinetic energy and distance through the precursor gas as well as the transit time through the gas, L/V, can be calculated. For example, 251 KeV beta electrons with a velocity of 0.743c have a time of flight, or transit time, of 2.2 ns though 50 cm of argon gas.

Substituting Eq. 33 into Eq. 4 provides the decrease in beta velocity with distance travelled through the gas:

(34) $$V(x) = c * \mathrm{sqrt}(KE_n^2(x) + 2\, KE_n(x) * m_o c^2) / (KE_n(x) + m_o c^2)$$

The CSDA length, L, from Table 4 is 50.0 cm, 27.5 cm, and 19.2 cm respectively for Ar, Kr, and Xe gas. The corrected KEn values and velocities V(x) for x=0 (the point just outside the tube wall) are listed in Table 6.

Table 6. Kr-85 Beta Electron Kinetic Energy and Velocity After Radioisotope Tube Loss Correction

KE(KeV) Initial Decay Energy	SPm (MeV-cm^2/gm)	ΔKEm (KeV)* loss	KEn(KeV) Corrected energy	V(KE)/c	V(KEn))/c corrected
251 ave.	1.83	63.5	187	0.743	0.682
687 max.	1.43	49.6	637	0.950	0.896

* V(KE) at x=0, $\Delta KE_m = 1.42 * SP_m * \rho_m * T_m$,Tm=0.005 cm, ρ_m =4.5 gm/cm^3

The V(x) decrease with KEn(x) over the distance L is illustrated in Fig. 7 for argon, krypton, and xenon gases.

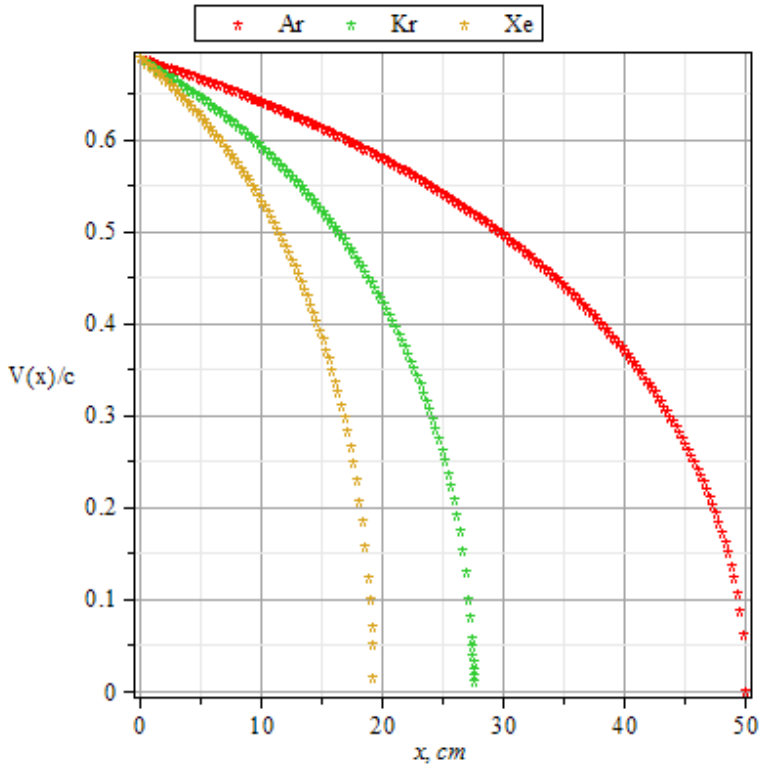

Fig. 7. Beta electron velocity V(x)/c versus distance through argon, krypton, and xenon gases. V(0)=0.682*c for the 187 KeV initial decay energy.

The minimum transient time through argon with the corrected kinetic energy and velocity, is 0.5m/0.682c or 2.37 ns. Integrating the reciprocal of the velocity decrease, V(x), over the 50 cm distance through the argon gas yields a total gas transit time of 209 ns.

This decrease in beta velocity through the gas also decreases the beta trajectory radius:

(35) $$R(x) = m_o V_{\perp}(x)/qB$$

As shown in Fig. 8b, the radius decrease, adjusted for emission angles, produces spiral rather than helical beta trajectories through the gas.

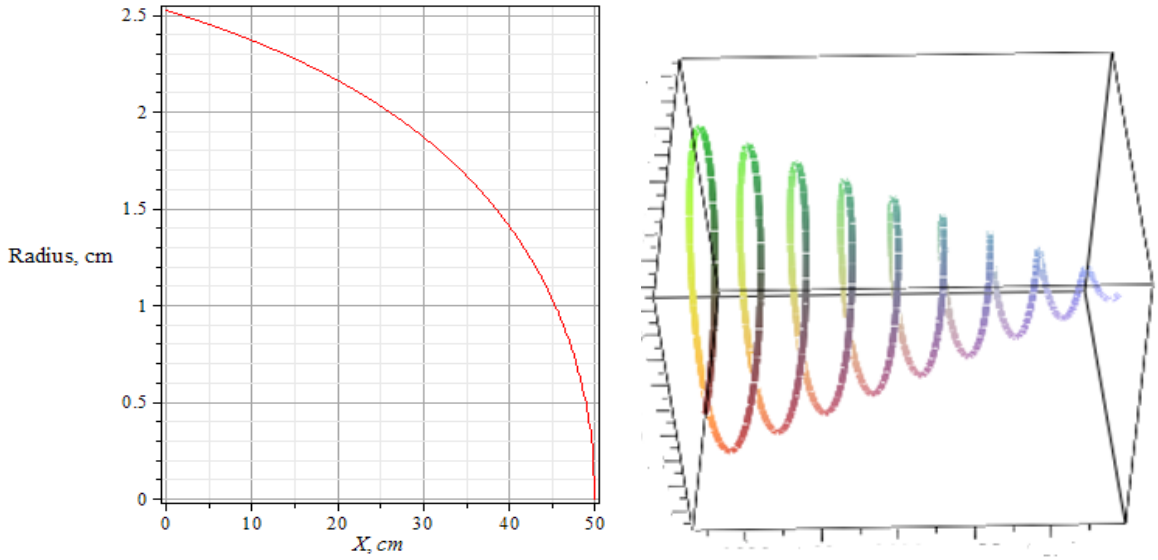

Fig. 8 (a) Decrease in spiral radius with distance through argon. (b) Beta spiral trajectory through gas.

5. Device Electrical Power

Substituting Eq. 28 for the net corrected beta kinetic energy, KE_n, along with Eq. 30 for the percentage of beta electrons passing through the tube, B%, provides the net beta power available for excimer generation:

(36) $$P_n = A(t)*B\%*KE_n$$

or

(37) $$P_n = A(t)*(2*(\Phi_{max} - \Phi_{min})/360) *(KE – (SP_m*\rho_m *T_m/ \sin(\Phi)))$$

For emission angles of 15 to 165 degrees, a Tm of 0.005 cm, density of 4.5 gm/cm3, KE_n of 187 KeV (2.99e-14 J/beta), and an initial A(t) of 1.45e13 beta/sec-gm, Eq.37 simplifies to:

(38) $P_n = 1.45e13*0.83*2.99e\text{-}14 = 0.361$ (beta watts/gm of radioisotope)

Multiplying P_n by the beta to photon power efficiency, η_{ex}, provides the excimer photon power:

(39) $P_{n\text{-}ph} = P_n*\eta_{ex} = 0.361*0.4 = 0.144$ (photon watts/gm of radioisotope)

The device electrical power can be generated from the photon power output, $P_{n\text{-}ph}$, with photovoltaic cells surrounding the excimer light tube. Wideband-gap photovoltaic cells, such as GaP, 6H-SiC, or doped diamond, with respective band-gaps of 2.3, 3.0, and 5.5eV, can directly absorb excimer photons with energy near the band gap. From Eqs. 38 and 39, a 1000 Ci source with 187 KeV average beta energy would produce about 391 mW of excimer power or 46 mW of electrical power assuming η_{ex} of 0.4 and a 12% cell efficiency.

Alternatively, the excimer photons can be converted to visible wavelengths with phosphors coated on the excimer precursor gas tube. Phosphors such as Ba2Gd (BO3)2Cl:Dy^{3+} or Ca_5Cl:Mn, used in UV photon conversion to white light, have quantum efficiencies up to 90%. [14]. The visible wavelength photons would allow the use of high efficiency multi-junction photovoltaic cells, such as $GaInP_2$/GaAs/Ge, to generate electrical power. These multi-junction cells have 30% conversion efficiency [13]. With the phosphor modification, the electrical power from the device is:

(40) $$P_e = A(t)*B\%*KE_n*\eta_{ex}*\eta_{phos}*\eta_{pv}$$

where η_{phos} is the excimer photon to phosphor emission efficiency and η_{pv} is the photovoltaic cell efficiency.

Table 7 lists the electric power output from the device at several Kr-85 Curie loadings. The Table calculations use an excimer to beta power output efficiency of 40%, phosphor quantum efficiency of 90% , and triple junction photovoltaic cell efficiency of 30%.

Table 7. Electrical Power Output for 251 KeV Beta Electrons with %B=1.

Kr-85 Gas (grams)	Curies	Beta Emission Rate (Beta/sec)	P, Beta electron Power (mW) A(t)*KE	P_{ph}, Excimer Photon Power (mW) ηex = 40%	P_e ,Electrical Power (mW) *
0.025	10	3.7e11	14.9	5.9	1.6
0.254	100	3.7e12	149	59	16
2.544	1000	3.7 e 13	1486	594	160.5
7.927	3111	1.15e14	4629	1852	500
15.856	6232	2.31e14	9260	3704	1000

* η_{ex} = 0.40, η_{phos} =0.9, η_{pv}=0.30.

From Table 7, the device output is about 0.160 milliwatt/Ci or 63.08 mW/gm of Kr-85. The device could deliver 500 mW of power with 7.9 grams or 3111 Curies of Kr-85 in the radioisotope tube.

The overall device conversion efficiency is:

(41) $$\eta = P_e / P_n = \eta_{ex}*\eta_{phos}*\eta_{pv}$$

With the Table 7 data, the device efficiency is (0.160 mW/1.49 mW) or 10.8%. Integrating the power over one half-life (10.7 years) yields a device specific energy of $5.91x10^6$ watt-hour per kilogram of Kr-85.

Table 8. Electrical Power Output for 187 KeV Beta Electrons with %B=0.83

Kr-85 Gas (grams)	Curies	Beta Emission Rate (Beta/sec)	P_n ,Beta electron Power (mW) $A(t)*KE_n$	$P_{n\text{-}ph}$,Excimer Photon Power (mW) $\eta ex = 40\%$	Electrical Power (mW) *
0.025	10	3.7e11	9.8	3.91	1.1
0.254	100	3.7e12	98	39	10.6
2.544	1000	3.7 e 13	978	391	105.6
12.77	4736	1.15e14	4629	1852	500
24.54	9472	2.31e14	9260	3704	1000

* $\eta ex = 0.40$, $\eta_{phos} = 0.9$, $\eta pv = 0.30$.

Table 9. Energy Loss and Activity Modified Electrical Power Compared to Base Case

	KE(KeV) Initial kinetic energy	An/Ao=%B Beta flux correction	mW/gm Specific power	mW/Ci	Efficiency %	Specific Energy (Wh/Kg)*
Base case	251	1.0	63.07	0.160	10.8 (0.160/1.49)	5.91e6
Corrected	187	0.833	39.37	0.100	10.8 (0.106/0.978)	3.69e6

* for specific power integrated over one half life (10.7 years)

6. Device Dimensions and Improvements

6.1 Dimensions with Kr-85

After including the beta energy losses, summarized in Table 9, an estimate of the component dimensions for the device in Fig. 2 can be calculated. From Table 8, a device that produces 105 mW of electrical power would require 1000 Ci of Kr-85. Kr-85 gas, pressurized to 18 atm at 20^o C, contains 25 Ci/ cm^3. Hence, a titanium tube with a volume of 40 cm^3 is required to hold the 1000 Ci. This volume requires a tube length of 15.7 cm, outer diameter, OD, of 1.8 cm, and wall thickness, Tm, of 0.005 cm. A tube burst pressure of 19.1 atmospheres is calculated from 2*Ts*Tm/OD. Ts is the titanium tensile strength. As discussed in Section 4, Kr-85 decays to Rb-85 which decreases the gas pressure in the sealed tube over time. The rate of decrease is slow and proportional to the Kr-85 decay activity, A(t). Since the tube burst (and crush) strength is 19 atmospheres, the tube will not collapse as the Kr-85 pressure decreases.

The diameter for the transparent excimer precursor gas tube, concentric to the titanium tube, depends on the magnetic field strength confining the trajectories of the beta electrons emitted through the titanium tube walls. Although the beta electrons quickly lose energy in the precursor gas, which decreases their trajectory radii, the maximum transparent tube radius will be estimated with Eq. 6, for the radius in vacuum at the initial beta energy. In vacuum, a magnetic field of 0.05 T along the tube axis produces an initial Kr-85 beta trajectory radius (at a 90^o emission angle) of 2.32 cm for the 187 KeV energy beta electrons. From Eq.7, the average radius for the 187 KeV electrons emitted through the titanium tube would be about 1.55 times the 90^o radius or 3.6 cm. The 90^o radius for the low number of

637 KeV beta electrons at the end of the Kr-85 spectrum is 3.0 cm and 1.55*3.0 or 4.65 cm when averaged over all emission angles. Choosing a 5 cm radius for the transparent tube, provides a gas tube cross section area (minus the Ti tube area) of about 76 cm^2 and volume of 1216 cm^3 for a 16 cm tube length. Filling this precursor gas tube to a pressure of 1 atm with Xe or a mixture of Xe and NF_3 would produce for Xe_2*or XeF*excimers as the betas pass through the gas. The data in Table 5, show the CSDA beta spiral trajectory path length in Xe is about 19 cm.

Surrounding this excimer photon emitting component with photovoltaic panels converts the photons to electrical power. The panel materials may also act as a radiation shield. Flexible thin film photovoltaic materials could also be wrapped around the outside of the transparent precursor gas tube as an alternative to the photovoltaic panels.

6.2 Device Improvements

To improve the device performance, several changes could be made. The most important change is to reduce the energy loss in passing through the titanium tube walls. As shown in Eq. 25, the tube wall loss, ΔKE_m, is proportional to $SP_m*\rho_m$. A 60% decrease in this energy loss can be achieved by substituting lower density aluminum for the titanium tube material with the same wall thickness. SP_m is similar for both metals. Substituting aluminum for titanium reduces the density, $\rho_{m,}$ to 2.7 from 4.5 gm/cm^3. As shown in Section 4.2, ΔKE_m is 41 KeV for the titanium tube wall loss. For an aluminum tube wall of the same thickness, ΔKE_m is 24.6 KeV. As shown in Eq. 26, multiplying this energy loss by 1.55 provides the average energy loss of about 38 KeV for all emission angles through the aluminum tube. The burst pressure of aluminum 6000 alloy is 17.2 versus 19.1 for titanium. Dropping the Kr-85 pressure to 16 atm requires increasing the tube volume to 1.125*40 cm^3 or 45 cm^3. This requires increasing the tube length to 17.7 cm. By changing the tube material, the beta electrons exiting through the aluminum tube have an average energy of 251-38 or 213 KeV versus 187 KeV for the titanium tube. Substituting this 213 KeV beta kinetic energy for 187 KeV in Table 8, increases the electric power to 120 mW from 105 mW.

The pressure within the tube could be greatly reduced by absorbing the Kr-85 gas on zeolite powder. This would allow very thin wall tubes. The trade-off is that the zeolites, with a stopping power similar to aluminum, would absorb some beta energy. Finally, if a very compact power source is required, the titanium or aluminum tube dimensions could be changed to accommodate liquid Kr-85 (-153 C) that contains 945 Ci/cm^3.

For solid radioisotopes, such as Pm-147 or P-32, the radioisotope gas tube, and its energy losses, can be eliminated. The solid radioisotopes can be coated on the outer surface of a small diameter tube or wire axially aligned with the magnetic field.

6.3 Secondary Electrons and Device Efficiency

Beta electrons inside the titanium tube and those passing through the tube walls can produce secondary electrons. Outside the titanium tube, the beta energy is mostly consumed by losses in the precursor gas. However, some beta electrons could impact the outside of the tube, metal magnets, or phosphors to produce secondary electrons. Since some secondary electrons could have energies greater than an excimer energy, they could generate additional photons and increase the device efficiency. However, at the present stage of the device development it is premature to estimate the increase.

A review of secondary electrons for primary electrons up to 50 KeV, has a secondary yield factor for titanium of 1.2. [19]. This article includes escape depths and yield dependence on primary energy. For titanium, the maximum yield energy is at 25 eV [15]. Hence, there is a lower probability for beta electrons with energy more than 25 eV to produce secondary electrons that will escape from the metal. The escape depth is a function of the stopping power of the material. An estimate of the maximum yield depth in titanium can be calculated from Eq. (25) for the stopping power energy loss. Substituting a ΔKE_m of 25 eV and $SP_m*\rho_m$ equal to 8.1 MeV-cm for titanium, the depth is 20 nm.

A rough estimate of the number of secondary electrons produced in the device can be calculated by multiplying the radioisotope specific activity, A(t) by the ratio of $\Delta KE_m/KE_n$. For the Kr-85 251 KeV beta electrons this ratio is about 10e-4. Until the amount of secondary producing surface area in the device is known, it is not possible to further estimate the number of secondary electrons or their energies.

8. Conclusions

This beta radioisotope power source provides a method to generate mW to watt levels of electrical power. The approach overcomes the power generation limitations of betavoltaic cells by magnetically confining beta electrons to spiral trajectories through excimer precursor gases. This allows very high radioisotope loading of the device (>1000 Ci) without damaging the device materials or surrounding photovoltaic cells. The magnetic beta confinement also reduces radiation shielding of the radioisotope.

The device power output is a function of the radioisotope loading, beta energy, beta flux, excimer precursor gas composition, and photovoltaic efficiency. Independent control of the beta flux with the magnetic field, Kr-85 gas pressure, and excimer precursor gas pressure can be used to optimize the photon generation and power output. The device is calculated to have a beta electron power to electrical power efficiency of 10.8 %. The maximum specific power is 63 mW per gram of Kr-85 or 0.160 mW/Ci. The specific energy is 5.91×10^6 Wh/Kg of Kr-85 over a 10.7 year half-life. Note that these specific power and energy metrics are based on the radioisotope mass only. They will need to be modified once the weight of other device components, photovoltaic panels, and radiation shielding are included.

The power source can use a variety of radioisotopes such as Kr-85, P-32, and Pm-147, can operate over a wide temperature range, and scales by stacking the devices within the photovoltaic enclosure to provide watt level power generation. In addition to remote power applications, the device can utilize Kr-85 off-gas from acid dissolution of spent nuclear fuel rod pellets at reprocessing plants or from accelerator driven sub-critical fission reactors to generate auxiliary power [16].

Acknowledgements

This work was funded in part by United States Department of Energy Grant DE-SC0012057.

References

[1] Revankar, S. and Adams, T, J. Advances in Betavoltaic Power Sources, *Power Energy Power Sources*, **1**, 321-329 (2014)

[2] City Labs Inc. Nanotritium Betavoltaic Cell ,www.citylabs.net

[3] Prelas, M., Boody, F., Miley,G., and Kunze,F. Nuclear Driven Flash Lamps, *Laser and Particle Beams*, **6**, (1), 25-62 (1988)

[4] Prelas,M., Charlson, E.J., Boody, F.P., Miley, G.H. Advanced Nuclear Energy Conversion Using a Two Step Photon Intermediate Technique. *Prog. In Nucl. Energy*, **23** (3), 223-240 (1990).

[5] Humphries, S., Charged Particle Beams, Wiley (1990).

[6] Bittencourt, J.A. Fundamentals of Plasma Physics, Ch. 2, Springer (2004)

[7] Sauerbrey, R. , Walter, W., Tittel, F.K., and Wilson, W.L. Kinetic Processes of Electron Beam Generated XeF* and Xe_2F* Excimers. *Journal of Chemical Physics*, **78**, 735 (1983)

[8] Neeser, S. Kunz, T., and Langhoff, H. A Kinetic Model for the Formation of Ar2 Excimers, *J. Phys. D. Appl. Phys*. **30,** 1488-1498 (1997)

[9] Wieser, J., Murnick, D. E., Ulrich, A., Huggins, H. A., Liddle, A., and Brown, W. L. Vacuum Ultraviolet Rare Gas Excimer Light Source. *Rev. Sci. Instrum* 1360 (1997)

[10] Ulrich, A., Heindl, T., Krucken, R.,Morozov, A., Skrobol, C., and Wieser,J. Electron Beam Induced Light Emission. *European Physical Journal:Applied Physics,* **47,** 1-4, (2009)

[11] Dandl, T., Hagn, H., Heindl, T., Krucken, R., Wieser, J. , and Ulrich, A. , Electron Beam Ignited High Frequency Driven Vacuum Ultraviolet Excimer Light Source. *Europhysics Letters*, **94**, No. 5 (2011).

[12] National Institute of Standards, ESTAR Data, physics.nist.gov /PhysRefData/Star/ Text/ ESTAR.html

[13] McConnell, R. and Symko-Davies,M. , Multijunction Photovoltaic Technologies for High Performance Concentrators, *IEEE 4th World Conference on Photovoltaic Energy Conversion*, NREL/PR-520-39866, (2006).

[14] Zhao,L. Wang, D. , Wang, Y., Bright White-Emitting Phosphors for Hg-Free Lamps and White LED Applications, *J. Am. Ceram. Soc.* **98**,1195 (2015).

[15] Lin,Y. and Joy, D., A New Examinatin of Secondary Electron Yield Data, Surf. Interface Anal., **37**, 895-900, (2005).

[16] Accelerator Driven Nuclear Energy, world-nuclear.org/information-library/current-and-future-generation/accelerator-driven-nuclear-energy.aspx (2016)